

Electrochemical Properties and Thin-Film Morphology of Mn-doped TiO₂ Thin Layer Prepared by Electrodeposition Technique and Its application as photocatalyst for Rhodamine B degradation

Jiarong Bi, Xiaoming Cao*

School of Materials Science and Engineering, Hebei University of Technology, Tian Jin 300401, China

*E-mail: gd-sam@21cn.com

Received: 29 November 2020 / Accepted: 8 January 2021 / Published: 31 January 2021

This study was conducted to investigate the Mn concentration effect as dopant on morphological, structural, electrochemical and photocatalytic properties of Mn-doped TiO₂ thin films. The pure TiO₂ and Mn-doped TiO₂ thin films were synthesized through electrodeposition method and XRD, SEM, electrochemical and photodegradation analyses were applied for characterization of synthesized thin films. XRD results showed the pure TiO₂ and Mn-doped TiO₂ thin films were deposited in anatase phase of TiO₂ and TiO₂ nanocrystal sizes were slightly decreased with the increasing of dopant concentration. SEM analysis showed that the pure TiO₂ and Mn-doped TiO₂ thin films were synthesized in relatively dense, highly homogenous, porous and highly effective specific surface areas of nanoparticles on substrates. The electrochemical studies exhibited that Mn doping lead to decrease of recombination rate of photogenerated electron-hole pairs which can be related to creation defects as electroactive and photoactive sites in electrodeposited film through doping process. Results also showed the presence of Mn could narrow the band gap of doped films which promotes photoactivity of TiO₂ films in visible light range. EIS study results showed that the smallest resistance of charge transfer was belonging to TiO₂: Mn (5%) thin film. Results of photodegradation analyses for degradation of RhB under sunlight irradiation displayed that the all Mn-doped TiO₂ thin films showed more degradation efficiency than pure TiO₂ and the photocatalytic performance of films was improved with increasing Mn concentration up 5% and best degradation efficiency was obtained for TiO₂: Mn (5%) thin film (99% degradation efficiency under 120 minutes sunlight irradiation) due to hinder the recombination of photogenerated holes and electrons. Therefore, the appropriate amount of Mn in TiO₂ thin film was obtained in TiO₂: Mn (5%) thin film for electrochemical and photoelectrochemical performance.

Keywords: Mn-doped TiO₂ thin films; Electrodeposition; Electrochemical impedance spectroscopy; Photodegradation; Photocatalyst

1. INTRODUCTION

TiO₂ is a most applicant semiconductor material in paint, sunscreen and UV blocking pigment in cosmetic, food coloring, photo-catalysts, dye sensitized solar cells, corrosive-protection coatings, solid state hydrogen storage devices, gas sensors, electrochemical sensors, batteries and electrochromic devices due to its high chemical and mechanical stability, inexpensive, low toxicity and *eco*-friendly [1, 2]. Studies showed that synthesis nanostructured TiO₂ thin films and modification of TiO₂ structures through doping or preparation TiO₂ based composites can be optimized the TiO₂ electrochemical performance in corrosive-protection films, sensors, solar cells, Li-ion batteries and photocatalysts [3, 4].

Accordingly, many studies were conducted for optimization synthesize methods of different nanostructures of TiO₂ such as nanotubes, nanoparticles, nanofibers, nanobelts, nanowires, nanoholes and nanorods [5, 6]. For example, anodic oxidative hydrolysis, physical vapor deposition, chemical vapor deposition, micelle and reverse micelle methods, direct oxidation, sonochemical, sol-gel, hydrothermal/solvothermal and electrodeposition are considered as well-known methods for synthesis of TiO₂ nanostructures [7]. Among them, electrodeposition has frequently been used an old technique for large area preparation of heterojunctions, heterostructures, multilayers and doped nanostructured semiconductors and metallic thin films because of low cost, simplicity and control in all of electrodeposition condition for preparation desirable nanomaterials in substrate and template [8, 9]. Therefore, this technique can control the morphology, thickness, density, stoichiometry and doping process by adjusting electrodeposition time, current and voltage and electrolyte concentration, pH and temperature.

Doping process is performed to improve the physical and chemical properties of TiO₂ such as stability, optical, electronic and photocatalytic properties by incorporation of various elements in semiconductor structure and change the surface pattern because of the creation of new energy levels near the conduction band, structural defects and distortion of crystal lattice [10-12]. Moreover, doping process is one of the band gap engineering methods which are a great factor for determination of semiconductor photo-activation region under a wide range of irradiated wavelength [13-15]. For example, photo-activation region of TiO₂ is limited to UV region due to its band gap value (3.3 eV) and doping with S, N, Cr, Cu, Ag, Fe, Mo, Al, Ni, V, W and Zn lead to narrowing the band gap and increases the activity to under visible light irradiation [16].

Therefore, this study was focused on effect of the Mn concentration as dopant on morphology, structure, electrochemical and photocatalytic properties of Mn-doped TiO₂ thin films.

2. EXPERIMENT

2.1. Synthesize of Mn-doped TiO₂ thin films

Mn-doped TiO₂ films was deposited on a glassy carbon electrode (GCE) through electrodeposition method in an electrodeposition cell which contained the GCE (3.0 mm diameter,

MF-2012, BASi, USA) as cathode and platinum wire as anode. The electrodeposition electrolyte was prepared of mixture aqueous solution of 0.20 M TiCl_4 (99.9%, Sigma-Aldrich, UK) and 3%, 5%, and 10% molar ratio of MnCl_2 (>99.0%, Sigma-Aldrich, UK) as known TiO_2 : Mn (3%), TiO_2 : Mn (5%) and TiO_2 : Mn (10%), respectively. Prior to the electrochemical deposition, the GCE was polished for 30 minutes on a prepared polishing kit which containing the mixture of 0.5 mg alumina slurry (0.5-1 μm , Henan Union Precision Material Co., Ltd., China) and 1ml deionized water. Then, the polished electrode was rinsed with deionized water and transferred to the electrodeposition cell. The electrodeposition process was carried out on cleaned GCE for 40 minutes under 0.4 V and constant current of $20 \mu\text{A cm}^{-2}$ as electrodeposition voltage, respectively. After deposition, the deposited Mn-doped TiO_2 film on GCE was washed by deionized water and dried at room temperature.

2.2. Characterization and measurement techniques

The scanning electron microscopy (SEM, FIB-SEM 40 CrossBeam Zeiss Auriga, Carl Zeiss, Jena, Germany) was used for study of morphology of electrodeposited Mn-doped TiO_2 thin films. X-ray diffraction (XRD, Rigaku D/Max 2200 X, Japan) was applied at power of 30 kV/20 mA and wavelength of $\text{CuK}\alpha$ ($\lambda=1.5418 \text{ \AA}$) for study the crystal phase structures of electrodeposited films. Electrochemical impedance spectroscopy (EIS) and cycle voltammetry (CV) measurements were carried out with AUTOLAB electrochemical workstation (Metrohm Autolab B.V., The Netherlands) in three-electrode electrochemical cell that Ag/AgCl, Pt and the electrodeposited thin films were applied as the reference, counter and working electrodes, respectively. The electrochemical measurements were conducted in 0.1 M Na_2SO_4 (99%, Shanghai Sky Chem Industrial Co., Ltd., China) solution as an electrolyte in electrochemical cell. Transient photocurrent measurements were conducted on bias voltage of 0.5V vs. Ag/AgCl. Photodegradation measurements were performed on the electrodeposited thin films as photocatalyst in the test chamber. The 10 mg/l solution of rhodamine B (RhB, $\geq 95\%$, Sigma-Aldrich) was prepared for photodegradation analyses. Optical absorbance spectra of photodegraded samples were measured by UV-Vis diffuse reflectance spectrometer (UV-Vis DRS: TU-1901, China) in the test chamber. The degradation efficiency (%) was calculated from the equation (1) [17, 18]:

$$\text{Degradation efficiency} = \left(1 - \frac{I}{I_0}\right) \times 100 = \left(1 - \frac{C}{C_0}\right) \times 100 \quad (1)$$

Where, I_0 is the initial absorption intensity and I is the photodegraded absorption intensity of dye solution. C_0 and C also refer to the initial and residual concentration of photodegraded dye solution, respectively.

3. RESULTS AND DISCUSSION

3.1. Structural and morphological studies of pure TiO₂ and Mn-doped TiO₂ thin films

X-ray diffraction patterns of pure TiO₂, TiO₂: Mn (3%), TiO₂: Mn (5%) and TiO₂: Mn (10%) powders were used to determine the created phase structure in the electrodeposition process. As observed in Figure 1, the recorded diffraction peaks at $2\theta = 25.29^\circ$, 37.89° , 48.04° , 53.88° and 55.06° , corresponding to (101), (004), (200), (105) and (211) planes (JCPDS Card No. 78-2486), respectively. All of the recorded diffraction peaks for pure TiO₂ and Mn-doped TiO₂ thin films were assigned to the anatase phase of TiO₂. As seen, with the increasing concentration of Mn, the width of the diffraction peak at $2\theta=25.29^\circ$ is slightly increased. Scherrer equation [10] was used to calculation of created nanocrystal sizes in thin films for strongest diffraction peak at $2\theta = 25.29^\circ$ which shows that nanocrystal sizes of pure TiO₂, TiO₂: Mn (3%), TiO₂: Mn (5%) and TiO₂: Mn (10%) are obtained 7.4, 7.1, 7.0 and 7.2 nm, respectively. Thus, TiO₂ nanocrystal sizes are slightly decreased with the increase of dopant concentration. Moreover, the recorded X-ray diffraction patterns did not show any oxide phase of MnTiO_x and Mn_xO_y which might imply that Mn²⁺ is incorporated into the TiO₂ lattice and good dispersion of the Mn²⁺ on the TiO₂ surface [19] that it is similar to the reports of Deng et al. [20] for study of Mn-doped TiO₂ nanoparticles.

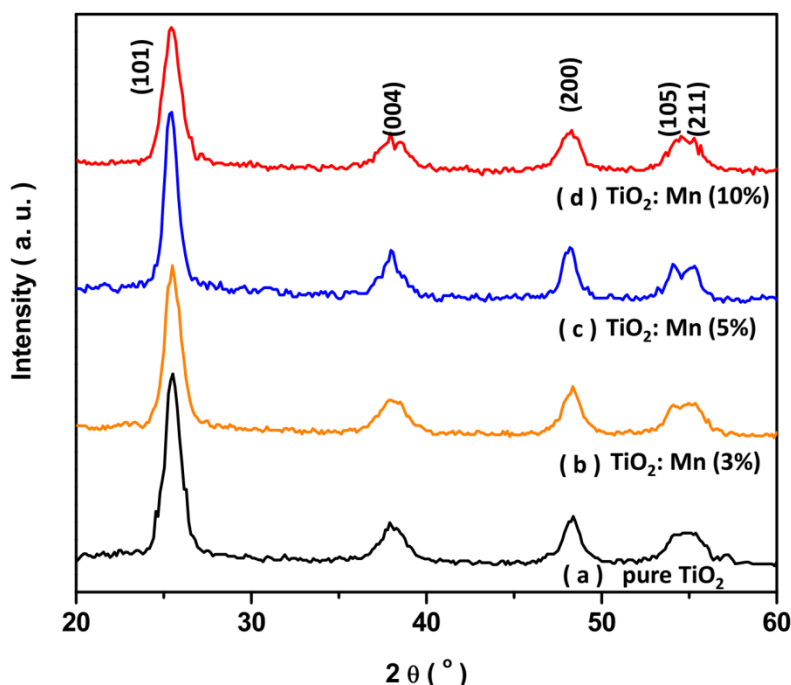


Figure 1. The recorded X-ray diffraction patterns of (a) pure TiO₂, (b) TiO₂: Mn (3%), (c) TiO₂: Mn (5%) and (d) TiO₂: Mn (10%).

Surface morphology of prepared thin films was studied through SEM analyses. Figure 2 shows SEM images of pure TiO₂ and Mn-doped TiO₂ thin films that exhibit the deposition of relatively dense, highly homogenous and porous nanoparticles on substrates. These morphological properties

indicate the promotion of the electrochemical property of prepared films because displays the high effective specific surface area.

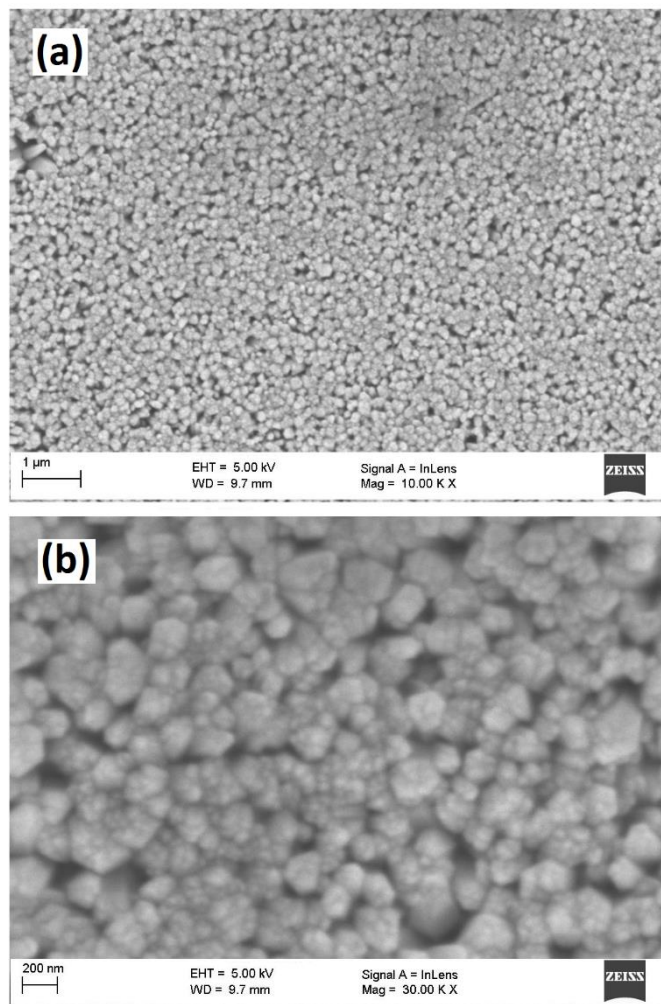


Figure 2. The SEM images of (a) pure TiO₂, (b) TiO₂: Mn (5%)

3.2. Electrochemical properties of the pure TiO₂ and Mn-doped TiO₂ thin films

The electrochemical properties of the pure TiO₂ and Mn-doped TiO₂ thin films were characterized by CV and EIS techniques. Figure 3 displays the recorded CVs of pure TiO₂ and Mn-doped TiO₂ thin films at scan rates of 100 mV s⁻¹ in potential range from -0.1 to 0.7 V in . There is the antisymmetric rectangular shape for recorded CV curves of pure TiO₂ film in Figure 3 that is implying the remarkable role of electrical double-layer capacitance to accumulation of charges. As observed in Figure 3, the shape of recorded CVs of Mn-doped TiO₂ thin films are changed to distorted rectangular shape. The distorted rectangular shape of the CV curves is evidence of desirable capacitive property of Mn-doped TiO₂ thin films which can facilitate faradaic charge transfer on modified GCE surfaces. Furthermore, with the increasing dopant concentration up 5%, the surrounding area of the CVs are increased and it is decreased for more increasing the Mn content in TiO₂ film (TiO₂: Mn (10%)). It is suggested that this is associated with the synergetic effect between the dopant and TiO₂

nanostructures [21]. Moreover, with the increasing Mn concentration, conductivity and capacitive values can be improved due to presence of free electrons of Mn conduction band [22]. While, increasing Mn concentration more than 5% lead to create defects in anatase TiO₂ structure and more mutual condensation reaction of hydroxyl groups on electrode surface which can decrease the effective specific surface area and as a consequence it can decrease the electric double-layer capacitance [23]. Moreover, increasing Mn concentration to 5% leads to enhancement of the current of recorded CVs which indicates that the TiO₂: Mn (5%) film shows great capacitive value.

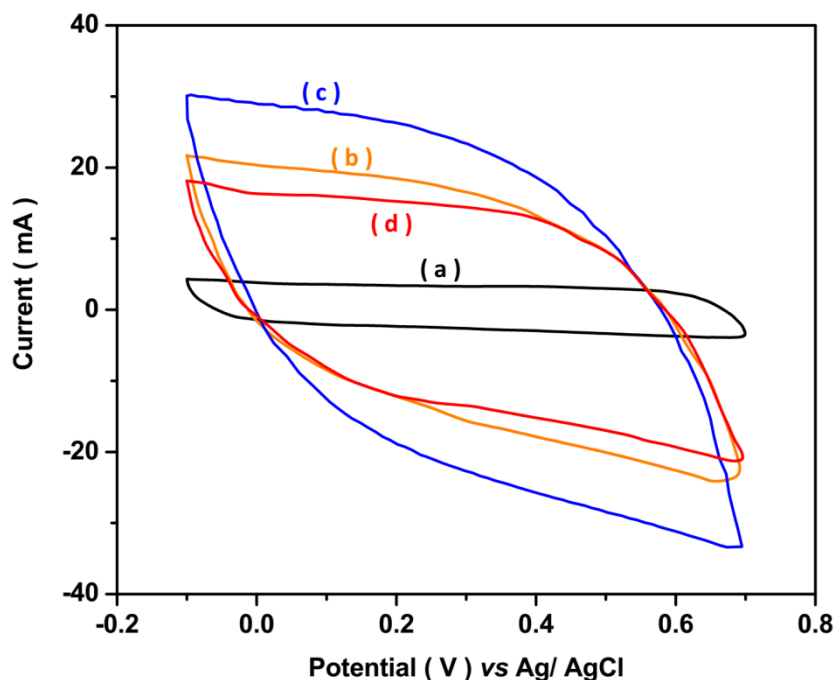


Figure 3. The recorded CVs of (a) pure TiO₂, (b) TiO₂: Mn (3%), (c) TiO₂: Mn (5%) and (d) TiO₂: Mn (10%) on GCE films in 0.5 M Na₂SO₄ at scan rates of 100 mV s⁻¹ with potential range from -0.1 to 0.7 V.

The stability effect of prepared electrodes was studied through the recorded successive CVs. Figure 4 shows the initial, 100th and 150th recorded CVs of pure TiO₂ and Mn-doped TiO₂ thin films on GCE. As seen, the changes of current after 100 sweeps are obtained 26, 8, 4 and 8% for pure TiO₂, TiO₂: Mn (3%), TiO₂: Mn (5%) and TiO₂: Mn (10%) films, respectively. In addition, changes current after 150 sweeps are 60, 18, 8 and 17% for pure TiO₂, TiO₂: Mn (3%), TiO₂: Mn (5%) and TiO₂: Mn (10%) films, respectively. These changes show that all Mn-doped TiO₂ thin films exhibit the stable electrochemical behavior and most stability treatment is obtained for TiO₂: Mn (5%) film.

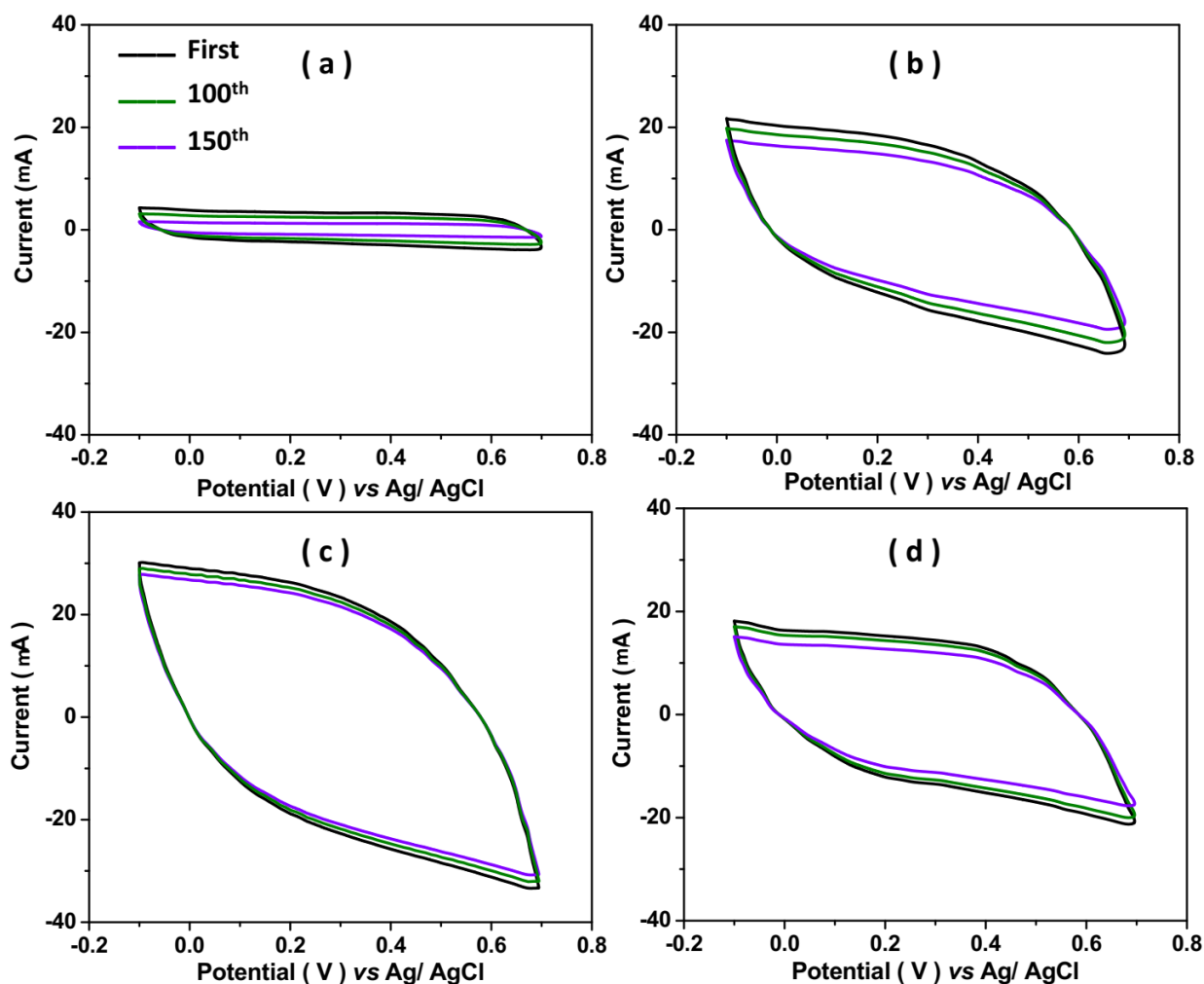


Figure 4. The initial, 100th and 150th recorded CVs of (a) pure TiO₂, (b) TiO₂: Mn (3%), (c) TiO₂: Mn (5%) and (d) TiO₂: Mn (10%) on GCE films in 0.5 M Na₂SO₄ at scan rates of 100 mV s⁻¹ with potential range from -0.1 to 0.7 V.

3.3. Photo-electrochemical properties of the pure TiO₂ and Mn-doped TiO₂ thin films

EIS measurements were carried out for clarifying the capacitance performance and electron transfer of prepared thin films at open circuit potential (OCP) and frequencies range from 10⁻¹ Hz to 10⁶ Hz with alternating current amplitude of 5Mv under sunlight illumination. Figure 5 shows the impedance Nyquist plots and equivalent circuit of electrodeposited films. By considering this point that large semicircle radius typically displays the large charge transfer resistance and high rate of recombination of photogenerated charges in semiconductor band gap [24-26], in Figure 5 is observed semicircle radius of pure TiO₂ film is larger than Mn-doped TiO₂ films which implying to Mn doping leads to decrease of recombination rate of photogenerated electron-hole pairs that can be related to creation of defects in electrodeposited film through doping process. The created defects can act as the great interfacial area and form more electroactive and photoactive sites for thin film. Furthermore, the presence of Mn could narrow the band gap of doped films which promotes photo-activation of TiO₂ films in visible light range [27]. It must be considered that the reduction of grain size on Mn-doped

film refers to formation of high specific effective surface areas [28, 29]. Moreover, interpolation and proportionate amount on Mn in TiO₂ lattice forms intermediate bands which have stepping stones that role for the photogenerated of charges under light irradiation and facilitate the transfer rate of excited carriers to the surface of film [30]. There is the smallest semicircle radius for TiO₂: Mn (5%) thin film that it illustrates the smallest resistance of charge transfer for film. It can see that TiO₂: Mn (10%) thin film shows largest semicircle radius and largest charge transfer resistance between the Mn-doped TiO₂ thin films.

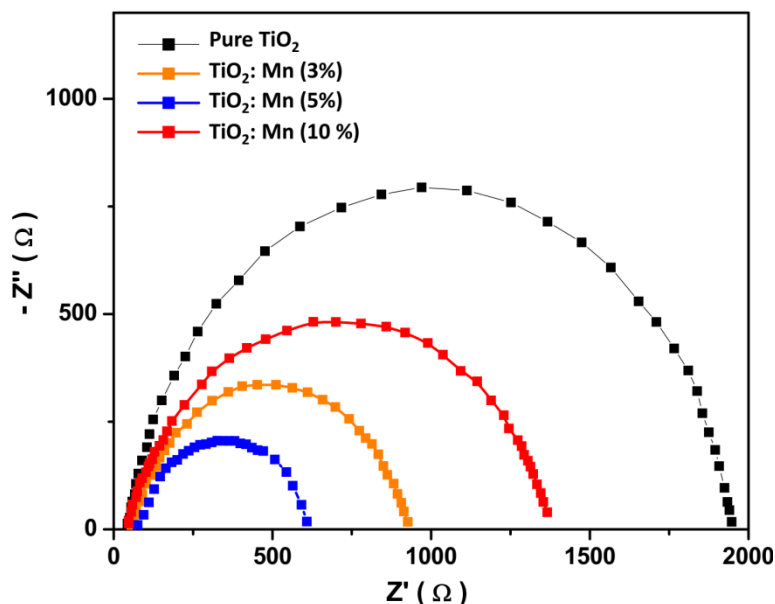


Figure 5. The recorded *impedance* Nyquist plots and equivalent circuit of pure TiO₂, TiO₂: Mn (3%), TiO₂: Mn (5%) and TiO₂: Mn (10%).

Further investigation for generation of photocurrent, transfer and recombination processes of charges carried out on study of transient photocurrent of prepared films. Figure 6 depicts the transient photocurrent response of pure and Mn-doped TiO₂ thin films under visible light irradiation. As observed, the photocurrent of Mn-doped TiO₂ thin films are higher than pure TiO₂ thin film. In these analyses can see the reduction of electron-hole recombination is the significant factor for enhancement of the transient photocurrent response of Mn-doped TiO₂ thin films because the highest photocurrent is belonging to the TiO₂: Mn (5%) thin film. It is considerable the photocurrent of TiO₂: Mn (10%) thin film is more than pure TiO₂ thin film and less than other Mn-doped TiO₂ thin films in this study. Therefore, TiO₂: Mn (5%) thin film possesses the appropriate amount of Mn in TiO₂ thin film. An other considerable point in Figure 6 are fast response and stable treatments of prepared electrodes to periodicon and off of light sources. As shown, all prepared electrodes exhibit fast response to present and absent light sources. Moreover, pure TiO₂ and TiO₂: Mn (3%) thin films show more stability responses under irradiation of light.

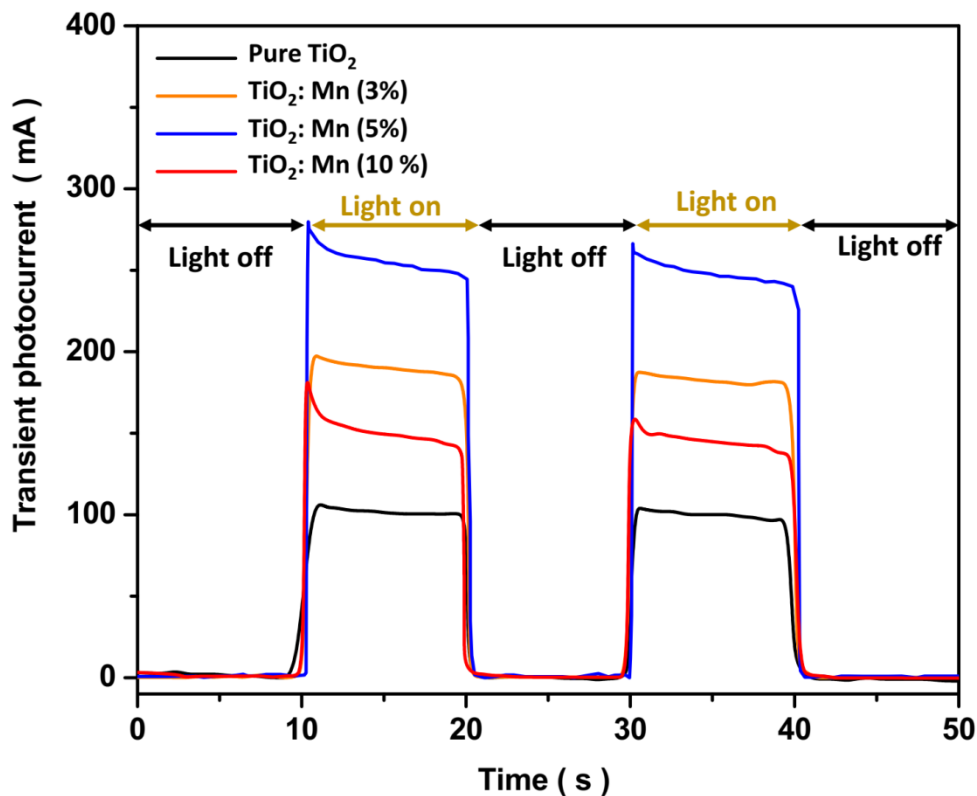


Figure 6. The recorded transient photocurrent response of pure and Mn-doped TiO₂ thin films under visible light irradiation.

3.4. Photocatalytic properties of the pure TiO₂ and Mn-doped TiO₂ thin films

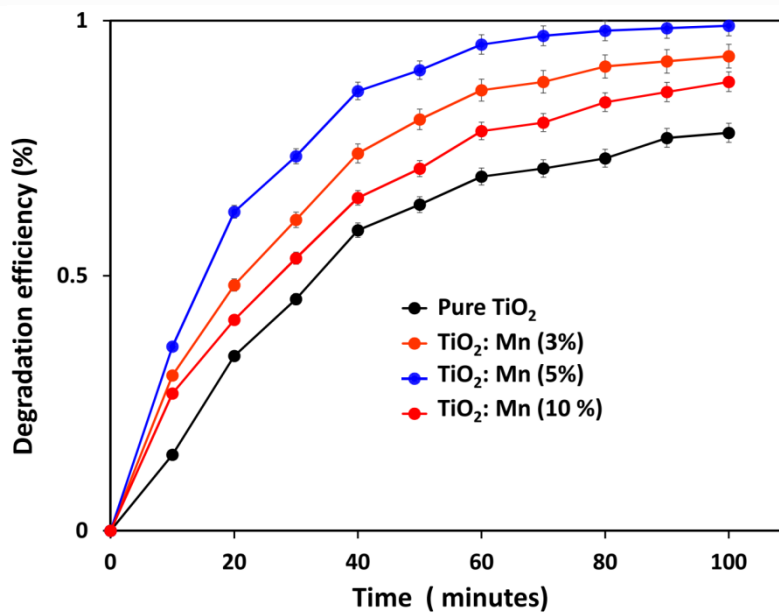


Figure 7. The recorded degradation efficiency of pure and Mn-doped TiO₂ thin films for degradation of RhB under sunlight irradiation.

The photocatalytic activity of pure TiO₂ and Mn-doped TiO₂ thin films was studied for degradation of RhB under sunlight irradiation. Figure 7 displays the degradation efficiency of prepared thin films which demonstrate all Mn-doped TiO₂ thin films possess more degradation efficiency than pure TiO₂ under sunlight irradiation. As seen, the photocatalytic performance of films are improved within increasing Mn concentration up to 5% and best degradation efficiency is recorded for TiO₂: Mn (5%) thin film due to hinder the recombination of photogenerated holes and electrons [31]. The degradation efficiency of TiO₂: Mn (10%) thin film is less than TiO₂: Mn (5%) and TiO₂: Mn (3%) thin films and more than pure TiO₂ thin film. It is suggested that this decrease of degradation efficiency in high concentration of Mn dopant in TiO₂ lattice can be attributed to dissipation of the internal energy within Mn ions [32].

Table 1 shows a comparison of between the prepared TiO₂: Mn (5%) thin film in this study and other reported literature based on Ti and TiO₂ photocatalyst for degradation of RhB. By considering the degradation time and amount of RhB, the electrodeposited TiO₂: Mn (5%) thin film shows better or comparable photocatalytic performance.

Table 1. Comparison of between the degradation performance of photocatalyst based on Ti and TiO₂ for degradation of RhB.

Catalyst	Synthesis method	Amount of RhB (mg/l)	Light source	Degradation efficiency (%)	Degradation time (minute)	ref
Titanosilicate/g-C ₃ N ₄ nanocomposite	Hydrothermal	5.0	Natural sunlight	99	40	[33]
Iodine doped TiO ₂ nanoparticles	Sol-gel	10.0	Natural sunlight	98	240	[34]
TiO ₂ (binary system)		5.0	Simulated sunlight	100	120	[35]
GeO ₂ /TiO ₂ nanoparticle composite	Solution Combustion	10.0	Natural sunlight	100	180	[36]
Graphene-TiO ₂ (P25) composite	Hydrothermal	8.6	UV light	65	60	[37]
Ce doped TiO ₂	Hydrothermal	0.5	UV light	80	120	[38]
P doped TiO ₂	Sol-gel	12	Solar light	85	40	[39]
TiO ₂ : Mn (5%) thin film	electrodeposition	10	Natural sunlight	99	100	This work

4. CONCLUSION

In this study pure TiO₂ and Mn-doped TiO₂ thin films were synthesized through electrodeposition method. The Mn concentration effects as dopant were studied on morphology, structure, electrochemical and photocatalytic properties of Mn-doped TiO₂ thin films. Results of structural study showed that pure TiO₂ and Mn-doped TiO₂ thin films were synthesized in anatase phase of TiO₂ and TiO₂ nanocrystal sizes were slightly decreased with the increasing of dopant concentration. Results of morphological study showed the deposition of relatively dense, highly homogenous, porous and highly effective specific surface area of doped and undoped TiO₂ nanoparticles on substrates. The results of electrochemical studies showed that Mn doping led to decrease of recombination rate of photogenerated electron-hole pairs due to creation defects in electrodeposited film through doping process. The created defects can act as the great interfacial area and form more electroactive and photoactive sites for thin film. Furthermore, the presence of Mn could narrow the band gap of doped films which promotes photoactivation properties of TiO₂ films in visible light range. It must be considered that the reduction of grain size on Mn-doped film refers to formation of high specific effective surface areas. Moreover, results showed that the smallest resistance of charge transfer was obtained for TiO₂: Mn (5%) thin film. Results of photocatalytic studies for degradation of RhB under sunlight irradiation showed that the all Mn-doped TiO₂ thin films had more degradation efficiency than pure TiO₂. In addition, the photocatalytic performance of films was improved with increasing Mn concentration up 5% and best degradation efficiency was obtained for TiO₂: Mn (5%) thin film due to hinder the recombination of photogenerated holes and electrons. Therefore, TiO₂: Mn (5%) thin film possesses the appropriate amount of Mn in TiO₂ thin film for electrochemical and photoelectrochemical performance.

ACKNOWLEDGEMENT

This work was sponsored in part by National Natural Science Foundation of China «Rare-earth-type fluxes improve the wetting mechanism of hot-dip high-aluminum-magnesium-zinc-based alloys and substrates» (51601056)

References

1. Y. Paz, *Applied Catalysis B: Environmental*, 99(2010)448.
2. H. Karimi-Maleh, Y. Orooji, A. Ayati, S. Qanbari, B. Tanhaei, F. Karimi, M. Alizadeh, J. Rouhi, L. Fu and M. Sillanpää, *Journal of Molecular Liquids*, (2020)115062.
3. M. Ge, J. Cai, J. Iocozzia, C. Cao, J. Huang, X. Zhang, J. Shen, S. Wang, S. Zhang and K.-Q. Zhang, *international journal of hydrogen energy*, 42(2017)8418.
4. M. Alimaneh, J. Rouhi and Z. Hassan, *Ceramics International*, 42(2016)5136.
5. M. Malekshahi Byranvand, A. Nemati Kharat, L. Fatholahi and Z. Malekshahi Beiranvand, *Journal of nanostructures*, 3(2013)1.
6. F. Tahernejad-Javazmi, M. Shabani-Nooshabadi and H. Karimi-Maleh, *Composites Part B: Engineering*, 172(2019)666.
7. S.V. Kuchibhatla, A. Karakoti, D. Bera and S. Seal, *Progress in materials science*, 52(2007)699.

8. Z. Savari, S. Soltanian, A. Noorbakhsh, A. Salimi, M. Najafi and P. Servati, *Sensors and Actuators B: Chemical*, 176(2013)335.
9. H. Karimi-Maleh, F. Karimi, M. Alizadeh and A.L. Sanati, *The Chemical Record*, 20(2020)682.
10. H. Savaloni and R. Savari, *Materials Chemistry and Physics*, 214(2018)402.
11. J. Rouhi, S. Mahmud, S. Hutagalung and S. Kakooei, *Micro & Nano Letters*, 7(2012)325.
12. R. Mohamed, J. Rouhi, M.F. Malek and A.S. Ismail, *International Journal of Electrochemical Science*, 11(2016)2197.
13. R. Hassanzadeh, A. Siabi-Garjan, H. Savaloni and R. Savari, *Materials Research Express*, 6(2019)106429.
14. J. Rouhi, S. Kakooei, S.M. Sadeghzadeh, O. Rouhi and R. Karimzadeh, *Journal of Solid State Electrochemistry*, 24(2020)1599.
15. A. Khodadadi, E. Faghih-Mirzaei, H. Karimi-Maleh, A. Abbaspourrad, S. Agarwal and V.K. Gupta, *Sensors and actuators b: chemical*, 284(2019)568.
16. V. Kumaravel, S. Mathew, J. Bartlett and S.C. Pillai, *Applied Catalysis B: Environmental*, 244(2019)1021.
17. A. Yi, Y. Feng, Z. Du and H. Li, *International Journal of Electrochemical Science*, 10(2015)1459.
18. C.-D. Dong, T.-S. Chen, C.-W. Chen and K.-L. Huang, *International Journal of Electrochemical Science*, 11(2016)5009.
19. H. Abdelouahab Reddam, R. Elmail, S.C. Lloria, G. Monrós Tomás, Z.A. Reddam and F. Coloma-Pascual, *Boletín de la Sociedad Española de Cerámica y Vidrio*, 59(2020)138.
20. Q. Deng, X. Xia, M. Guo, Y. Gao and G. Shao, *Materials Letters*, 65(2011)2051.
21. M.M. Momeni, M. Hakimian and A. Kazempour, *Ceramics International*, 41(2015)13692.
22. W. LuXihong, *NanoLetters*, 12(2012)1690G1696.
23. A. Zhang, Z. Zhang, J. Chen, W. Sheng, L. Sun and J. Xiang, *Fuel Processing Technology*, 135(2015)25.
24. Y. Yang, X. Huang, Y. Yang, C. Wu, B. Lei, Q. Peng and G. Wang, *International Journal of Electrochemical Science*, 14(2019)3673.
25. Y. Li, J. Sun, J. Wang and S. Xia, *International Journal of Electrochemical Science*, 13(2018)11454.
26. G. Liu, Y. Zhang, M. Wu, Y. Zhang and B. Pang, *International Journal of Electrochemical Science*, 13(2018)6248.
27. L. Wang, X. Zhang, P. Zhang, Z. Cao and J. Hu, *Journal of Saudi Chemical Society*, 19(2015)595.
28. I. Habib, A.A. Tajuddin, H.A. Noor, C.M. Lim, A.H. Mahadi and N. Kumara, *Scientific reports*, 9(2019)1.
29. F. Chahshouri, H. Savaloni, E. Khani and R. Savari, *Journal of Micromechanics and Microengineering*, 30(2020)075001.
30. G. Shao, *The Journal of Physical Chemistry C*, 113(2009)6800.
31. N. Sharotri, D. Sharma and D. Sud, *Journal of Materials Research and Technology*, 8(2019)3995.
32. M. Xue, L. Huang, J.-Q. Wang, Y. Wang, L. Gao, J.-h. Zhu and Z.-G. Zou, *Nanotechnology*, 19(2008)185604.
33. A.K. Adepu, R. Anumula and V. Narayanan, *Microporous and Mesoporous Materials*, 247(2017)86.
34. R.P. Barkul, M.K. Patil, S.M. Patil, V.B. Shevale and S.D. Delekar, *Journal of Photochemistry and Photobiology A: Chemistry*, 349(2017)138.
35. D. Ariyanti, M. Maillot and W. Gao, *Journal of environmental chemical engineering*, 6(2018)539.

36. K. Natarajan, H.C. Bajaj and R.J. Tayade, *Materials Chemistry Frontiers*, 2(2018)741.
37. H. Zhang, X. Lv, Y. Li, Y. Wang and J. Li, *ACS nano*, 4(2010)380.
38. J. Xiao, T. Peng, R. Li, Z. Peng and C. Yan, *Journal of Solid State Chemistry*, 179(2006)1161.
39. Y. Lv, L. Yu, H. Huang, H. Liu and Y. Feng, *Journal of Alloys and Compounds*, 488(2009)314.

© 2021 The Authors. Published by ESG (www.electrochemsci.org). This article is an open access article distributed under the terms and conditions of the Creative Commons Attribution license (<http://creativecommons.org/licenses/by/4.0/>).